Journal of Power Sources 247 (2014) 40–48

Contents lists available at ScienceDirect

Journal of Power Sources

journal homepage: www.elsevier.com/locate/jpowsour

Influence of cell temperature on sulfur dioxide contamination in proton exchange membrane fuel cells

Y. Zhai*, G. Bender [1], K. Bethune, R. Rocheleau

Hawaii Natural Energy Institute, University of Hawaii, Honolulu, HI 96822, USA

HIGHLIGHTS

- Lower temperature, less performance recovery was obtained by neat air operation.
- Full recovery was obtained by CV scanning after contamination at low temperature.
- Increase of liquid water in MEA delayed the poisoning process at low temperature.
- Decomposition/desorption of sulfur adsorbates was inhibited at low temperature.
- SO_2 crossover from cathode to anode was also mitigated at low temperature.

ARTICLE INFO

Article history:
Received 11 June 2013
Received in revised form
5 August 2013
Accepted 12 August 2013
Available online 30 August 2013

Keywords:
PEM fuel cell
Sulfur dioxide contamination
Electrochemical impedance spectroscopy
Cyclic voltammetry
Water balance

ABSTRACT

The effects of temperature on sulfur dioxide (SO_2) contamination in PEMFCs are investigated by operating single cells with 2 ppm SO_2 in the cathode at different temperatures. Cell performance response shows that voltage degradation was delayed and appears a transition of multiple processes at low temperatures; a similar performance loss is observed when performances reached steady state. The restored performance from the reversible and the irreversible degradations highly depends on temperature. At low temperature, the performance recovery is only negligible with neat air operation (self-recovery), while full recovery is observed after cyclic voltammetry (CV) scanning. As temperature increased, so did the self-recovery performance. However, the total recovery performance decreased. Electrochemical impedance spectroscopy analysis indicates that the potential-dependent poisoning process was delayed at low temperature, and the removal of the sulfur species from Pt/C was inhibited during the self-recovery. Water balance analysis implies that the delay could be attributed to the effect of liquid water scavenging and the mass transport of SO_2 in the membrane electrode assemblies. The CV analysis confirms that the decomposition/desorption of the sulfur adsorbates was inhibited and indicates that the SO_2 crossover from the cathode to the anode side was also mitigated at low temperature.

1. Introduction

Proton exchange membrane fuel cells (PEMFCs) have been considered one of the most promising clean energy technologies and suitable primary power sources [1]. Traces of impurities are known to exist in air, such as NO_x, SO_2, and organics. These impurities primarily originate from vehicle exhausts and industrial emissions, which can be introduced into the PEMFC cathode with air feeding streams. They can cause performance degradation and sometimes permanent damage to the membrane electrode assemblies (MEAs) [2–6]. To date, most of the cathode contamination studies focused on the effect of SO_2 on the degradation and recovery of PEMFC performance [6–18]. Severe degradation and a small partial slow self-recovery have been observed, and this finding is commonly accepted. The sulfur compounds adsorbed on the Pt surface tended to be oxidized to sulfate by CV scanning beginning at 0.9 V after they were reduced to adsorbed sulfur [10,16].

In our previous work, SO_2 contamination in PEMFC cathodes was observed to cause a multi-processes poisoning during constant current operation at 80 °C. The multiple poisoning processes result from: i) an irreversible adsorption of SO_2, which is independent of SO_2 concentration but depends on the coverage of the sulfur oxides; ii) a reversible adsorption of SO_2, which depended on the SO_2 concentration and the cathode potential; and iii) an anode

* Corresponding author. Tel.: +1 8085931714; fax: +1 8085931719.
E-mail address: yunfeng@hawaii.edu (Y. Zhai).
[1] Currently at National Renewable Energy Laboratory, Golden, CO 80401, USA.

0378-7753/$ – see front matter © 2013 Elsevier B.V. All rights reserved.
http://dx.doi.org/10.1016/j.jpowsour.2013.08.054

poisoning by SO_2 crossover through the MEA [15]. The performance loss caused by the reversible process could be recovered by neat air operation. However, the loss caused by the irreversible process could only partially be recovered by CV scanning at high potentials after the sulfur adsorbate was reduced to sulfur on Pt/C. The electrochemical impedance spectroscopy (EIS) analysis indicated that the reversible adsorption of SO_2 also assists the oxygen reduction reaction (ORR) processes shifting from a direct four-electron to a series two-electron pathway [18].

The SO_2 adsorption on Pt or Pt/C has been extensively studied by physical/chemical characterizations and theoretical methods [19–35]. The effect of SO_2 adsorption on the ORR was also studied by ex-situ CV and/or the rotating ring disk electrode method [36,37]. These works indicated that SO_2 can dissociate to sulfur and sulfur oxides on Pt/C [19,20] or can be reduced catalytically or electrochemically to sulfur in the absence of oxygen [21]. Pre-adsorbed sulfur on Pt would significantly block oxygen adsorption [22]. Other studies concluded that the adsorbed SO_2 can be catalytically oxidized into SO_3 or SO_4 by pre-adsorbed oxygen [22–28]. The adsorbed SO_3 or SO_4 on different Pt crystal structures can also dissociate into adsorbed SO_2 and O at different temperatures [22,29]. These works provided important initial insights to understand the mechanism of SO_2 contamination in PEMFCs under certain operating conditions. Furthermore, these results indicate that the oxidation–reduction reactions of SO_2 on the Pt surface are complicated and depend on the historic conditions and the reaction environment, such as the temperature [30], adsorbate coverage [26,29], potential of the Pt electrode [31,32] and absorption of oxygen on Pt [22–24]. These findings suggested that the SO_2 contamination in PEMFCs is a complicated process that strongly depends on the operating conditions.

As a candidate power source for practical applications, PEMFCs are operated at varying operating conditions. It is difficult to predict the impact of SO_2 on the PEMFC's performance before understanding the SO_2 contamination mechanism at realistic operating conditions. Furthermore, the impurity's access to the catalyst and the removal of the product rely on the diffusion through the GDL and catalyst layer in the cathode. The change in water content and the variation of water management at different operating conditions will play an important role. Therefore, the influence of operating conditions on SO_2 contamination in PEMFCs needs to be elucidated by experimental investigation.

In this work, SO_2 contamination experiments were performed in PEMFCs with 2 ppm SO_2 at different cell temperatures. SO_2 exposure was followed by recovery via neat air operation (self-recovery) and subsequent CV scanning (CV recovery). The PEMFCs were then re-exposed to SO_2 to determine the effectiveness of the recovery and gain insights into the re-poisoning processes. EIS analysis was used to determine the influence of the operating conditions on the SO_2 contamination in PEMFCs. Two factors should be taken into account when studying the effect of cell operating temperature: (i) the SO_2 adsorption, which directly impacts ORR; and (ii) the SO_2 mass transport, which directs how the contaminant reaches the catalyst and involves the diffusion of SO_2 through the air and water vapor in the gas diffusion layer (GDL), followed by the liquid water and Nafion film in catalyst layer (CL).

2. Experimental

Experiments were performed using an evaluation system, single cells and testing processes that have been previously described [15,18]. FCATS™ G050 series test stations (Green Light Power Technologies Inc.) were used with 50 cm^2 single-cell hardware. The anode flow-field had a double channel serpentine configuration, while the cathode flow-field had a triple channel serpentine

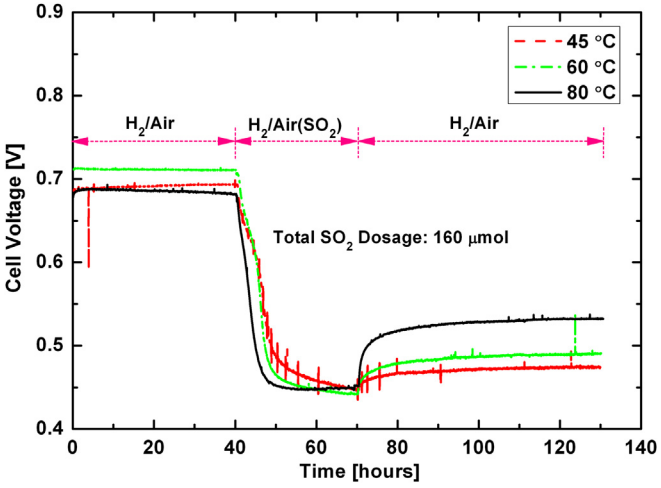

Fig. 1. Cell voltage changes with time during the 2 ppm SO_2 contamination experiments at different temperatures.

configuration. The MEA consisted of commercially available MEAs from Ion-Power Inc. with 0.4 mg Pt cm^{-2} loading and 50% Pt/C catalysts (KPTON® frame 50 cm^2, KPT-50, Lot#: 756). The cells were assembled with SIGRACET® SGL 25 BC gas diffusion layers (GDL) from SGL Technologies and PTFE gaskets on both the anode and cathode electrodes. The anode was fed with fully humidified (100% relative humidity, RH) H_2 and the cathode with 50% RH air; both the anode and cathode gas flow rates were maintained at a 2-fold stoichiometric ratio, current density of 0.6 A cm^{-2} and outlet back pressure of 48.3/48.3 kPa. A series of SO_2 contamination experiments were performed at cell temperatures of 45 °C, 60 °C, and 80 °C. A contaminant gas was injected into the humidified feed stream of the cathode to expose the PEMFC to SO_2. During this process, the humidification in the inlet gas was kept constant by increasing the temperature setting of the humidifier unit. The contaminant gas consisted of 93 ppm SO_2 in air (certified plus grade, Matheson Tri-Gas Inc.).

For the constant current operation (CCO) contamination experiment, PEMFCs were pre-poisoned for 40 h under neat H_2/air operation, followed by 30 h of 2 ppm SO_2 exposure and 60 h of self-induced performance recovery with neat H_2/air. All cells were operated at a current density of 0.6 A cm^{-2} during CCO. CV scanning was performed by switching to the H_2/N_2 operating mode with a Parstat 2273 from EG&G Instruments Corporation after cell activation and after CCO. Cell polarization curves were obtained before pre-poisoning and after CV recovery with neat H_2/air at the same operating conditions as those employed during CCO. During the polarization curves test, the cell was hold at the each set current density for 15 min (except 3 min for OCV). The cell voltage was recorded with an acquisition frequency of 1 Hz. Each MEA was again exposed to SO_2 for 20 h with operating parameters those used during the first exposure after a second pre-poisoning while operating with neat H_2/air for 20 h.

The CV scanning was conducted at 35 °C with fully humidified hydrogen or nitrogen in each side at a flow rate of 0.466 L min^{-1}. The hydrogen and nitrogen were supplied to the reference and working electrodes, respectively. A total of 16 scans were performed with a scan rate of 20 mV s^{-1}. The potential range of the first 13 cycles was 0.08–1.2 V vs. the hydrogen reference electrode (HRE), while that of cycles 14 to 16 was 0.08–1.5 V vs. HRE.

During the SO_2 contamination experiments, EISs from 10 kHz to 0.1 Hz (10 points per dec) were obtained with the ZPlot® (Scribner Associates) software with a Solartron SI1260 Impedance/Gain-

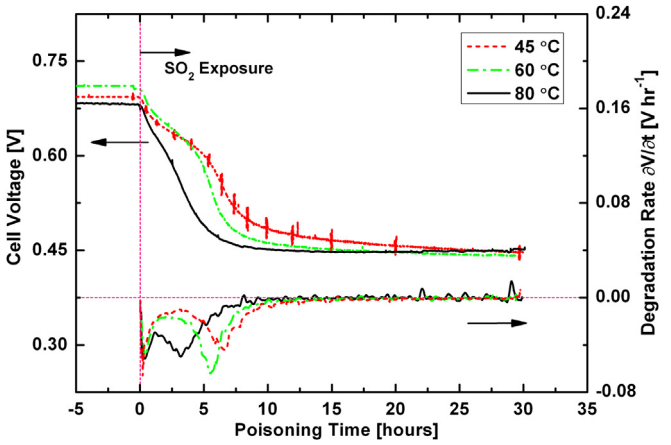

Fig. 2. Cell voltage degradation rate responses to the SO_2 exposure at different temperatures.

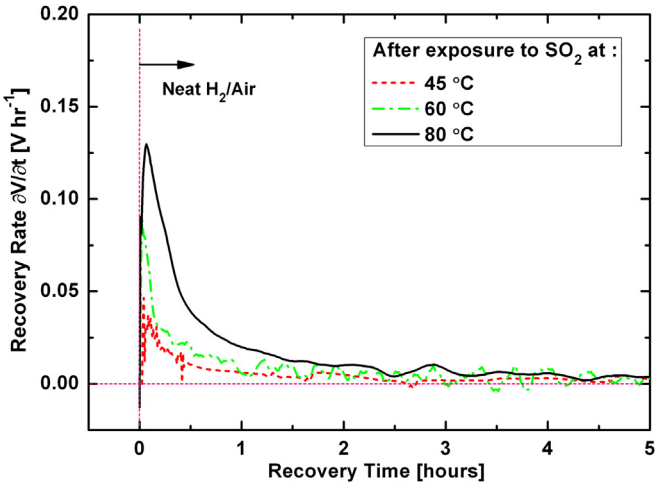

Fig. 3. Cell voltage recovery rates vs. time after exposure to 2 ppm SO_2 at different temperatures. The first 5 h are shown.

Phase Analyzer and Stanford Research SR560 Low Noise Pre-amplifiers. An AC current perturbation of 0.75 A was applied to the single cell during CCO with a DC current of 30 A.

Additionally, the water balance of the cell was investigated in identical experiments but without SO_2 contamination. The water in the cell outlet was condensed and collected with a condenser system. The temperatures and pressures at end of the humidifiers and the condensers were monitored. The water collection time was about 5–16 h for each condition. The flow rates of the inlet and outlet water were calculated form the averages of all the measured parameters. These results were used to calculate the neat water flux through the catalyst layers. The calculated mass balance of water in vs. water out for the cell is less than ±2%.

3. Results and discussion

3.1. Influence on cell performance degradation and recovery

The experiment results obtained at 80 °C and 2 ppm SO_2 in our previous work [15] were used as the reference basis for this study. Fig. 1 shows the change in cell voltage with operating time during CCO at different cell operating temperatures. During the first 40 h of operation with neat H_2/air, the performance of the cell at 45 °C increased by approximately 4 mV. However, the performances of the cells at 60 °C and 80 °C decreased by approximately 1 and 5 mV, respectively. These results can be attributed to the water produced by the cell reaction, which affects the humidity in the MEA cathode and water content in the membrane. The water-carrying capacity of the gas correlated positively with the temperature [38], which decreased the actual local RH in the catalyst layer. Additionally, increasing cell temperatures accelerated the normal cell performance degradation. Nevertheless, all MEAs reached steady states; the voltages were 0.694, 0.711 and 0.682 V at 45, 60 and 80 °C, respectively. After initiating SO_2 exposure, all cell voltages decreased rapidly within approximately 10 h to 0.486, 0.465 and 0.451 V for cells at 45, 60 and 80 °C, respectively. The cell voltage at 80 °C reached steady state after the initial rapid decline, but those at 60 °C and 45 °C continued to decrease at slower rates until the SO_2 injection was ceased. This effect was especially pronounced for the cell at 45 °C. After exposure to 160 μmol SO_2 (injection of 2 ppm SO_2 for 30 h), the cell voltages reduced to 0.447, 0.442 and 0.451 V for cells at 45, 60 and 80 °C, respectively. These values constituted 64.4%, 62.2% and 66.1% of the pre-poisoning performance of cells at 45, 60 and 80 °C, respectively. The cell voltage increased rapidly as soon as SO_2 injection was stopped and reached values of 0.463, 0.472 and 0.509 V for cells 45, 60 and 80 °C, respectively, after approximately 5 h self-recovery. The degree of voltage recovery correlated positively with cell operating temperature. After approximately 60 h of self-recovery, the voltages for cells at 45, 60 and 80 °C recovered to 0.474, 0.491 and 0.532 V, respectively. The increases in cell performances constitute approximately 10.9%, 18.2% and 35.1% of performance losses for cells at 45, 60 and 80 °C, respectively. The contamination experiment at 80 °C was repeated with a fresh MEA. The cell voltages during both tests showed less than 1% different, and the voltages losses were about 1% different. This comparison indicated the cell performance response was reproducible. The cell performance degradation processes during the exposure and the self-recovery processes will subsequently be discussed in detail.

Fig. 2 shows the cell voltage (top graphs, left *Y*-axis) and the voltage degradation rate (bottom graph, right *Y*-axis) vs the SO_2 exposure time at different cell operating temperatures. The voltage degradation rate in the time domain is the derivative of the cell voltages with respect to time, $\partial V/\partial t$. Two distinct peaks appeared in the voltage degradation rate curves that correspond to the two stages in these curves for all cells at different operating temperatures. These results agree very well with our previous work [15]. The initial portions of the cell performance degradation curves are similar at different operating temperature and all cells lost approximately 5% of their performance during the first a half hour of SO_2 exposure. The voltage degradation rates show similar initial peaks in the maximum degradation rate at approximately 50 mV h^{-1}. After the first peak, all voltage degradation rates decreased with continued SO_2 exposure; and the degradation rates decreased more slowly at high cell temperatures. Conversely, the voltage degradation rate increased with the cell operating temperature during the transient period between the two degradation peaks. However, the inflection point still appeared at approximately 0.63 V after 3.15, 3.00 and 1.26 h for cells at 45, 60 and 80 °C, respectively. This result suggested that the influence of cell operating temperature on the onset voltage of the reversible process was negligible. The transient period was extended and the cell performance degradation was inhibited as the cell operating temperature decreased. These phenomena clarified the two phases in the degradation curve when the cell was operated at low temperatures. For the second peak in the cell voltage degradation rate curve, the maximum degradation rate was approximately 44, 64

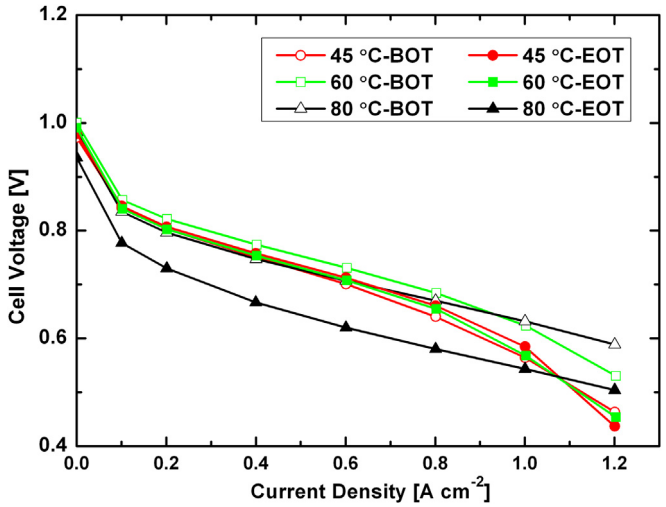

Fig. 4. Cell polarization curves before the tests shown in Fig. 1 and after CV recovery at different temperatures.

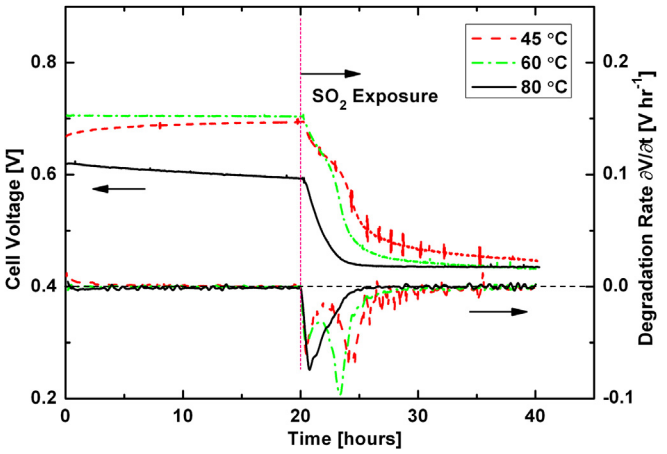

Fig. 5. Cell voltage response to the second SO_2 exposure and degradation rate at different temperatures.

and 50 mV h^{-1} for cells at 45, 60 and 80 °C, respectively. These peaks shifted from 6.66, 5.48 to 3.18 h as the temperature was increased from 45, 60 to 80 °C, respectively. After approximately 10 h, all cells experienced rapid, two-phase performance degradation, and the cell performance loss was approximately 30.2%, 35.1% and 33.7% for cells 45, 60 and 80 °C, respectively. After the two-phase degradation, the cell performance at 80 °C stabilized, but those at 60 and 45 °C continued to decrease by approximately 2.8% and 5.4%, respectively, during the last 20 h of exposure. These changes indicated the temperature did not significantly affect cell SO_2-induced performance loss, but that did significantly affect SO_2 contamination process.

Fig. 3 shows the cell voltage self-recovery rate, also defined as the derivative of the cell voltage with respect to time, $\partial V/\partial t$, during the first 5 h in neat H_2/air. The Figure shows that the voltage recovery rate of all cells was maximized as soon as SO_2 injection was stopped. The maximum values were 47, 89 and 146 mV h^{-1} for cells at 45, 60 and 80 °C, respectively. The recovery rates then decreased rapidly in all cases within the first hour for all experiments. These results indicated that the self-recovery of cell performance was significantly influenced by the cell operating temperature: the partial recovery and the recovery rate correlated positively with the temperature. This finding suggested that high cell temperatures benefited the self-recovery of the performance loss caused by the SO_2 contamination. As reported by Garsany et al., operating PBI-PEMFCs with neat air at 160 °C led to complete cell performance recovery from H_2S or SO_2 contamination [13]. This phenomenon should be attributed to the desorption of the sulfur species from the Pt surface at higher cell temperatures in the presence of adsorbed oxygen. SO_2 can desorb by two mechanisms, which start at approximately 27 °C and 145 °C in the presence of O_2 and correspond to weak and strong adsorption, respectively [30].

After self-recovery, CV scanning was used to analyze the irreversible SO_2 adsorption and further improve recovery until the CV curves overlapped. The polarization curve of the MEA was subsequently obtained at its experimental operating conditions and compared the curve obtained prior to contamination. The analysis of the irreversible SO_2 adsorption based on the CV data will be discussed in Section 3.2.2, and the polarization curves that were obtained prior to the contamination experiments and after CV recovery are shown in Fig. 4. The cell voltage was the average of values obtained within the last 5 min of the data acquisition period. The variation of the voltage in this period was less than 1 mV. A comparison of the cell performance before the contamination experiments at 80 °C to that after CV recovery indicates that the OCV of the MEA decreased from 0.983 to 0.936 V, which constitutes a decrease of approximately 50 mV. The cell performance also declined significantly at the active polarization zone and high current densities, and the decrease reached values of up to 90 mV. At 60 °C, the OCV decreased by approximately 10 mV; the performance declined by approximately 20 mV at current densities below 0.8 A cm^{-2}, and the mass transfer overpotential increased slightly at high current densities (>1 A cm^{-2}). However, at 45 °C, the OCV increased by approximately 10 mV and the MEA performance improved slightly at the current densities from 0.4 to 1.1 A cm^{-2}. This effect can be attributed to the decreased ohmic overpotential. A significant increase in mass transfer overpotential was observed at high current densities above 1 A cm^{-2}. The decrease in the OCV and cell performance implied permanent damage to the membrane and catalyst layer of the MEAs caused by SO_2 contamination, especially at 80 °C. The decrease in the ohmic overpotential and the increase in mass transfer overpotential at 45 °C indicated that the SO_2 contamination changed the properties or structure and the water management of the MEA. This change resulted in a little improvement in the cell performance after recovery. These results suggested that the lower cell temperature would likely significantly mitigate the permanent cell performance loss caused by SO_2 contamination. A more detailed study on the structural effects of SO_2 contamination on the MEA will be presented in the near future.

Fig. 5 shows the recovered cell performance, second SO_2 exposure and the cell voltage degradation rate at same operating conditions as those of the first exposure. The recovered cell performance correlated negatively with the cell temperature, i.e., 100% was recovered at 45 °C, 99.3% at 60 °C, and only 90.9% at 80 °C. The cell performance was completely recovered at lower cell temperature, while a 9% permanent loss was observed at 80 °C. The cell voltage degradation curves showed a clear two-phase process during the second exposure at 45 and 60 °C, but only one voltage degradation rate peak at 80 °C. This difference should be attributed to the potential-dependent SO_2 contamination process. When the cathode potential at the starting point of SO_2 injection was lower than the onset potential, i.e., the cell voltage was 0.63 V, the potential-dependent SO_2 contamination process occurred in parallel with the coverage-dependent SO_2 contamination process. This process would result in one peak on the degradation rate curve, like that for the cell at 80 °C. Correspondingly, the voltage degradation

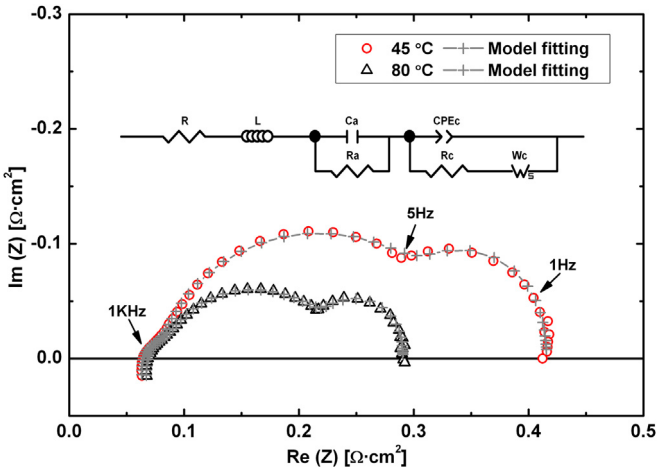

Fig. 6. A sample of the EIS from the cells at 45 °C and 80 °C as well the ECM simulation result.

rate has two peaks for 45 and 60 °C. At 45 °C, the peak values are 60 and 68 mV h^{-1}at 0.23 and 4.1 h of SO_2 exposure, respectively. At 60 °C, the peak values are 52 and 96 mV hr^{-1}at 0.23 and 3.1 h of SO_2 exposure, respectively. The single peak observed at 80 °C was at 74 mV hr^{-1}. During the second exposure, the maximum degradation rate of the concentration-dependent process increased 1.5-fold over the first exposure for both 45 and 60 °C; the exposure time to reach the peak was shortened by 61% and 57% for 45 and 60 °C, respectively. However, the cell performance approximates that of the first exposure when the cell contamination reaches steady state. These results suggested that the Nafion degradation caused by the SO_2 contamination might change the properties of the catalyst layer, such as the effective ionomer film area, and accelerate the mass transport of SO_2 to the catalysts [6,39].

3.2. Influence on impurity adsorption and transport

3.2.1. EIS analysis

EIS was employed to investigate the catalyst and mass transfer effect of SO_2 contamination on the MEAs at different cell temperatures. Fig. 6 shows a sample EIS at 45 and 80 °C before SO_2 exposure. There are three arcs on each EIS: the high frequency response is attributed to the hydrogen oxidation reaction (HOR), the mid frequency response to the oxygen reduction reaction (ORR) and the low frequency response to the mass transfer in the GDE. The value at which the EIS intersects with the Re (Z) axis at high frequencies represents the serial resistance of the proton and electron transport in the bulk system. The diameters of the arcs at high, median and low frequency ranges represent the HOR resistance, the ORR resistance and the mass transport resistance in the GDE, respectively. The EIS shows a slightly lower internal resistance at 45 °C compared to that observed at 80 °C. Conversely, the mass transport and ORR resistances were higher at the lower temperature. Both temperatures exhibited a similar HOR resistance. These differences can be explained by the higher water content in the MEA, lower ORR reaction rate and slower gases diffusions at lower temperature.

As described in a previous study [18], an equivalent electrical circuit model (ECM, insert of Fig. 6) was applied to simulate the impedance spectra by using the ZView® (Scribner Associates) software. The simulation results of the ECM fit well with the cell's experimental responses over the whole frequency range for all CCO periods. The ECM parameters R, L, Ra, Rc, Rd and Td, were extracted

Table 1
A sample of all the parameters obtained by the ECM fitting to the EIS obtained before SO_2 exposure (square symbol in Fig. 6).

Parameter	45 °C	Error [%]	80 °C	Error [%]
R [Ω cm^2]	0.0628	0.3	0.0667	0.3
L [H]	5.19E-09	2.2	5.47E-09	1.9
Ra [Ω cm^2]	0.0151	3.4	0.0138	4.8
Rc [Ω cm^2]	0.257	1.7	0.146	1.8
Rd [Ω cm^2]	0.0814	4.9	0.0640	3.5
Td [s]	0.201	2.5	0.173	2.1

from the software simulation. R represents the serial resistance of the protons and the electrons transport in the bulk system. L represents the inductance of the system. Ra stands for the anode charge transfer resistance of the HOR. Rc signifies the cathode charge transfer resistance of the ORR. Rd represents the gas diffusion resistance in the GDE, and the diffusion time constant, $Td = l^2/D$, is given by the effective diffusion thickness, l, and the effective diffusion coefficient of the reactant, D. The parameters show similar trends at 45 °C and at 80 °C, as mentioned in our previous work [18]. During the pre-poisoning tests, Rc dominates the reaction resistances for both cases, and R, Ra and Rd are much lower than Rc. The simulated parameter values from the EIS obtained before the exposure at 45 and 80 °C are shown in Table 1 as samples. Table 1 shows that a lower cell temperature resulted in reduced ohmic resistance but higher reaction resistances, diffusion resistance and a higher diffusion time constant. The cathode charge transfer resistance at 45 °C was approximately 76% higher than that at 80 °C. The slight decrease in the ohmic resistance could be related to the increased liquid water content in the MEA; the details will be discussed in Section 3.2.3. Furthermore, the increases in the reaction and diffusion resistances as well as the diffusion time constant can be explained by slower reaction dynamics and transport at lower temperatures.

No obvious changes in R, L or Ra were observed throughout the CCO. Therefore, only the variations in Rc and Rd at 45 °C and 80 °C during the SO_2 contamination and cell performance recovery were compared. The variations in Rc and Rd during the SO_2 contamination experiment at 80 °C have been previously discussed [18]. The variations at 45 °C are shown in Fig. 7. Rc and Rd were observed to increase rapidly within approximately 7.5 h of SO_2 exposure, reaching values of 1.111 and 0.431 Ω cm^2, respectively. These values

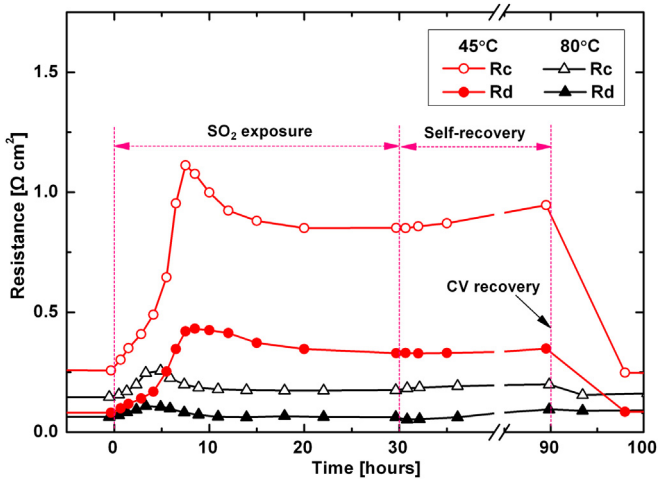

Fig. 7. The variation in the cathode charge transfer resistance, Rc, and cathode gas diffusion resistance, Rd, during the SO_2 exposure and cell performance recoveries at 45 °C and 80 °C.

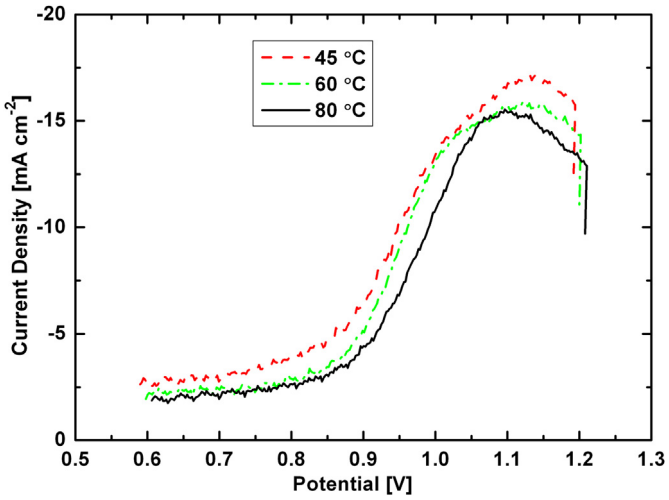

Fig. 8. The sulfur adsorbate oxidation curves during the first cathode CV cycle after the experiments shown in Fig. 1.

constitute a 430% increase in Rc and a 530% increase in Rd over their pre-exposure values. Then Rc and Rd started decreasing. After approximately 20 h of exposure, both reached stable values of 0.850 and 0.347 Ω cm^2 respectively. These variations in Rc and Rd should be attributed to the SO_2 contamination and the ORR pathway shift, such as in the process observed at 80 °C [18]. However, Rc or Rd did not noticeably change after SO_2 injection was ceased, even after 60 h of self-recovery; the Rc and Rd values were 0.946 and 0.348 Ω cm^2, respectively. These values constituted 3.7- and 4.3-fold increases over the initial values of Rc and Rd, respectively. These results correspond to the negligible cell performance restoration observed during self-recovery. Compared to 80 °C, the SO_2 contamination at 45 °C resulted in a more significant increase of Rc and Rd, which might be explained by the stronger adsorption of the sulfur adsorbate on Pt at lower temperature [21]. The negligible change in Rc or Rd during the self-recovery at 45 °C suggested that the desorption of the sulfur adsorbate, which occurred at 80 °C [18], was inhibited at lower cell temperature. The temperature effect on SO_2 desorption from Pt/C surface was also mentioned in the literature [30].

3.2.2. CV analysis

CV scanning was used to analyze the SO_2 adsorption and any additional recovery after self-recovery. Fig. 8 shows the sulfur species oxidation peak in the first CV curve of the cathode after the SO_2 contamination experiment (Fig. 1) at different cell operating temperatures. The CV profiles show a significant peak in the Pt oxide formation potential area at approximately 1.10, 1.12 and 1.13 V vs. HRE at 80, 60 and 45 °C, respectively. Furthermore, there is an obvious shoulder at approximately 1.02 V vs. HRE for cells at 45 and 60 °C. According to a previously published study [19], the oxidation peaks at 1.10, 1.12 and 1.13 V for the experiments at 80, 60 and 45 °C should be indicative of the electrochemical oxidation of adsorbed sulfur at the cathode. This result indicated that the oxidation current peaks of adsorbed sulfur slightly shifted to a higher potential when the sulfur species adsorbed to the Pt surface at lower cell temperatures. According to Mohtadi et al. [40,41], sulfur adsorbs more strongly at lower cell operating temperature when H_2S dissociates on the Pt surface in the anode of PEMFCs, which results in a shift in the oxidation current peaks of adsorbed sulfur to a slightly higher potential. Similarly, the adsorption and dissociation of sulfur oxides in the cell cathode may also result in stronger sulfur adsorption on the Pt surface at lower cell operating temperature.

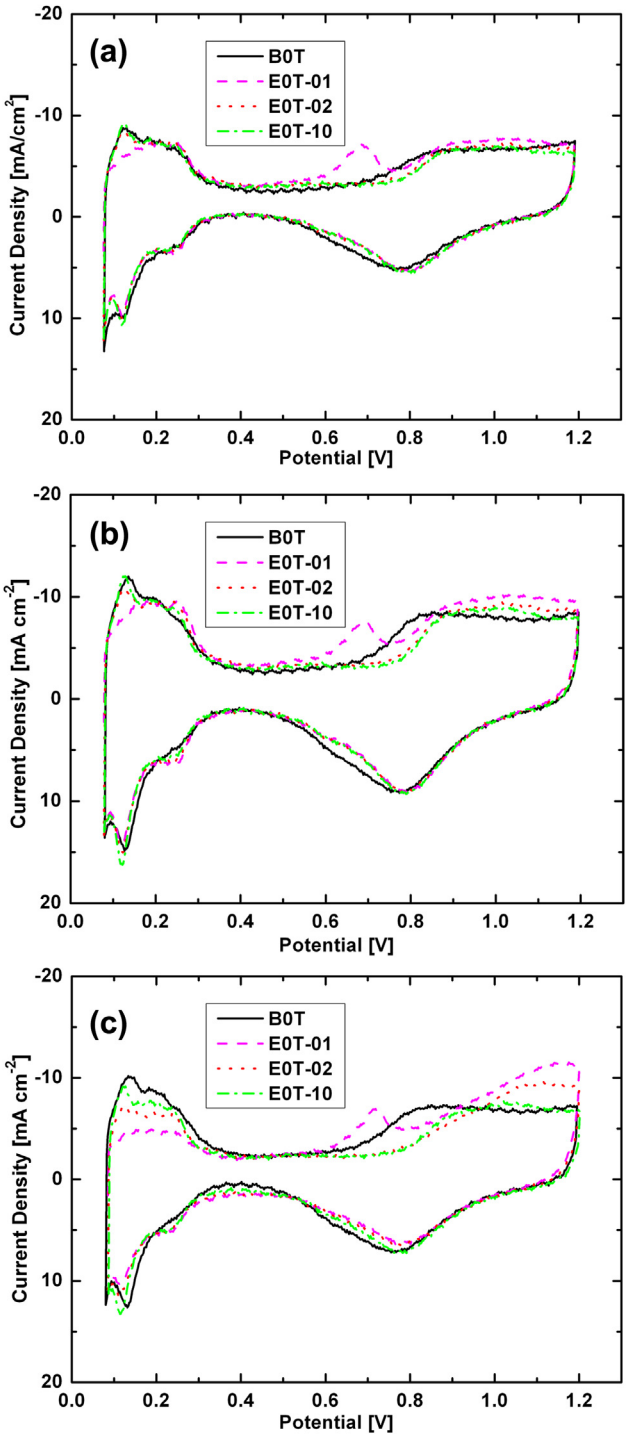

Fig. 9. Anode CV curves before and after the experiments shown in Fig. 1: (a) 45 °C, (b) 60 °C and (c) 80 °C. B0T: Beginning of Test; E0T: End of Test; −01: 1st cycle; −02: 2nd cycle; −10: 10th cycle stand for the steady cycles.

The additional shoulder in the oxidation peak suggests that an additional sulfur adsorbate with a different adsorption state remains on the Pt surface after the contamination and self-induced recovery experiments at 60 and 45 °C. The data in Fig. 8 also shows that the maximum current density of the sulfur oxidation peak increased as the experimental temperature of SO_2 contamination decreased. These results confirmed that the desorption of the sulfur adsorbate was inhibited by a lower cell operating

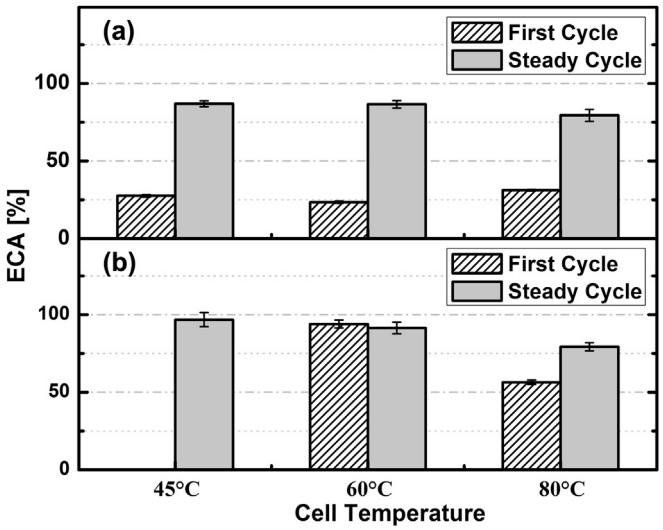

Fig. 10. ECA improvement at the cathode (a) and anode (b) by CV recovery after the experiments shown in Fig. 1.

temperature, which resulted in increased sulfur adsorbate retention on the catalyst surface of the cathode when the cell was operated after self-induced recovery at lower temperatures. The inhibition resulted in the reduced cell voltage self-recovery at lower operating temperatures.

Fig. 9 shows the anode CV curves of the cell contaminated at different temperatures: (a) 45 °C (b) 60 °C and (c) 80 °C. BOT is the steady cycle before the contamination experiment; EOT indicates that the CV curve was obtained after the contamination experiment: −01, −02, and −10 are the first, second, and steady cycles, respectively. It should be noted that Fig. 9(a) shows the anode EOT CV curves after the second exposure of the 45 °C experiment because those for the first exposure at 45 °C were interrupted unexpectedly. Furthermore, the peaks at approximately 0.7 V during the forward scanning of EOT-01 signify the oxidation of adsorbed CO, which originated from the purge with purified N_2 [15] and did not affect the comparison between the results at different temperatures. Fig. 9(a) and (b) show a slight decrease in the EOT-01 H_{ad} oxidation peak compared to BOT and a negligible sulfur adsorbate oxidation peak; EOT-10 does not show significant changes except for a shift in the onset potential of Pt oxidation. Fig. 9(c) shows a significant decrease in the EOT-01 H_{ad} oxidation peak and an obvious sulfur adsorbate oxidation peak; the EOT-10 also shows an increased shift in the onset potential of Pt oxidation. Comparing the data in Fig. 9(a)–(c), the sulfur oxidation peaks in the CV profiles showed that more sulfur adsorbed on the anode electrode at higher cell operating temperatures, and the increased shift implied that more sulfate anions were present on the anode side. These results indicated that the crossover of SO_2 from the cathode to the anode increased as the cell operating temperature increased. Generally, the gas permeability of the polymer electrolyte membrane (Nafion®) increased with temperature [42]. This phenomenon increases SO_2 crossover and then accelerates the SO_2 contamination in the anode. As indicated by the results in Fig. 2, the anode SO_2 contamination can reach a poisoning saturation state at higher temperatures, and this effect continued at lower temperatures even cathode contamination reached to its poisoning saturation state, especially at 45 °C.

The electrochemically active surface areas (ECAs) of the cathode and anode were determined by integrating the hydrogen oxidation desorption charges in the CV profiles. Fig. 10 shows the ECA changes of cathodes (a) and anodes (b) after contamination experiments

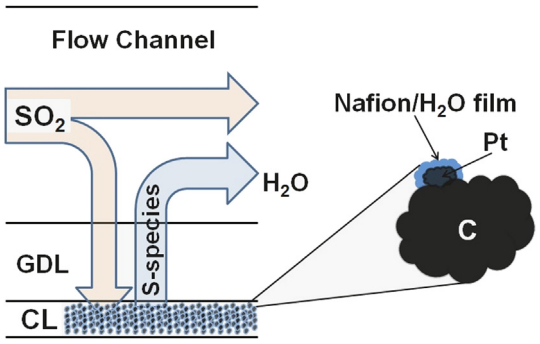

Fig. 11. Illustration of SO_2 mass transport in the cathode.

(Fig. 1) at different cell temperatures, such as the first cycle; and after CV induced recovery, such as the steady state cycle. It should be noted that, as mentioned above, the anode CV scanning of the 45 °C experiment was interrupted; anode ECA data were not collected for the first CV cycle at 45 °C in Fig. 10. All the percentage data were based on the ECA values at BOT. Fig. 10(a) shows that: (i) after self-induced recovery, a 72%, 76% and 69% ECA loss remains at the cathode for contamination experiments at 45, 60 and 80 °C, respectively; (ii) after CV recovery, the cathode ECA recovered approximately 88%, 87% and 80% for the MEA contaminated at 45, 60 and 80 °C, respectively. These results indicated self-recovery and cell temperature correlated positively; however, more CV recovery was observed in the cathode. The data in Fig. 10(b) show that: (i) after self-recovery, the anode had a 6% loss of ECA at 60 °C, this loss reached 44% at 80 °C; (ii) after CV recovery, the anode ECA recovered by approximately 97%, 91% and 79% for 45, 60 and 80 °C, respectively. These different results indicated that the SO_2 crossover is negligible at lower cell operating temperature, but severe at higher cell operating temperature. Additionally, higher cell temperatures also aggravated the permanent ECA loss by SO_2 contamination on both the cathode and anode sides.

3.2.3. Water balance analysis

The mass transport of SO_2 within the gas diffusion electrode (GDE), which is similar to that of oxygen, is illustrated in Fig. 11: the diffusion limitation in the gas phase is negligible compared to that in the liquid and solid phase due to the relatively large diffusion coefficient in the gas phase. As a result, the diffusion within the liquid water and Nafion® film in the CL controlled the transport processes of SO_2 to the catalysts. Therefore, the liquid water content in the cathode and the solubility of SO_2 would play important role in the access processes. Disregarding the complexity of the liquid water distribution and transport within the components of MEA, the total liquid water flux through the cathode GDL was estimated to analyze the effect of cell temperature on the mass transport of SO_2 by detecting the water balance under the identical operating conditions but without SO_2 contamination. Fig. 12(a) shows the schematic of H_2O transport in MEA and the average H_2O flow rates through the interfaces of CL and GDL in the anode and cathode, from anode to cathode was defined as the positive direction. Assuming the produced H_2O due to gas crossover was negligible, the H_2O sources include the inlet gases of the anode and cathode and the cell reaction in the cathode CL, as shown in the schematic. The total H_2O balance in the MEA can be described by Eq. (1):

$$\dot{n}_{V,in} + \dot{n}_F \approx \dot{n}_{L,out} + \dot{n}_{V,out} \quad (1)$$

Thus, the total average flow rate of the liquid water in the exhaust condensers (anode and cathode) can be calculated by Eq. (2):

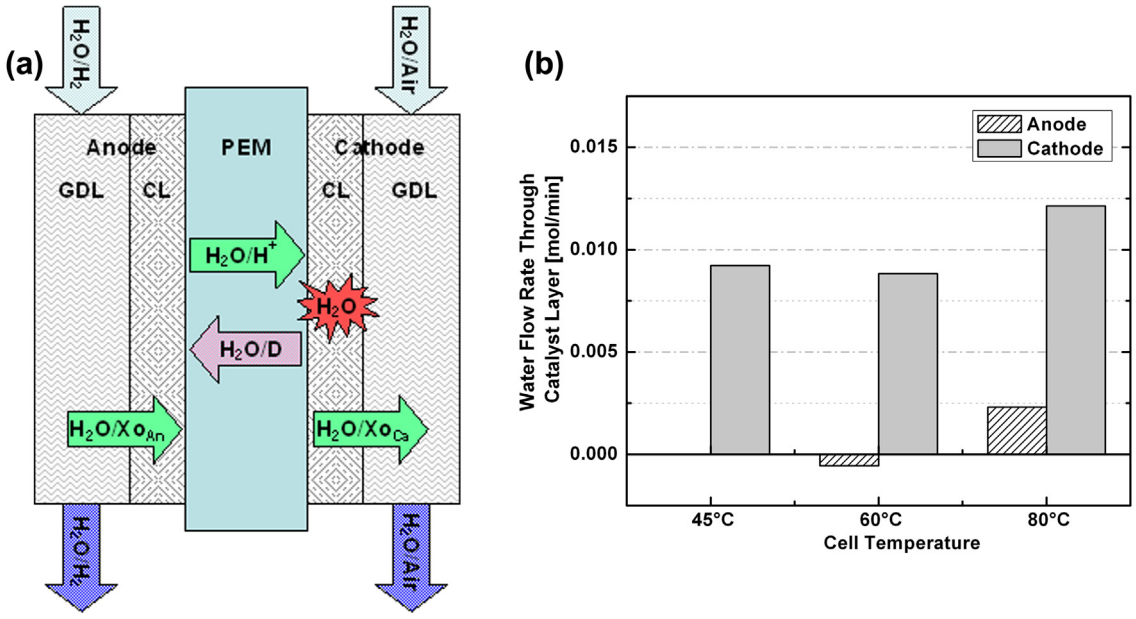

Fig. 12. (a) Schematic of the water transport in the MEA, and (b) the water balance in the MEA during the CCO at different cell temperature. The direction from the anode to the cathode was set as the positive direction.

$$\dot{n}_{L,out} \approx \dot{n}_{V,An,in} + \dot{n}_{V,Ca,in} + \dot{n}_F - \dot{n}_{V,An,out} - \dot{n}_{V,Ca,out} \quad (2)$$

The average H_2O flow rate through the CL is the difference between inlet and outlet, as shown in Eqs. (3) and (4):

$$\dot{n}_{An,xo} = \dot{n}_{V,An,in} - \dot{n}_{An,L,out} - \dot{n}_{An,V,out} \quad (3)$$

$$\dot{n}_{Ca,xo} = \dot{n}_{Ca,L,out} + \dot{n}_{Ca,V,out} - \dot{n}_{V,Ca,in} = \dot{n}_F + \dot{n}_{An,xo} \quad (4)$$

where $\dot{n}$ is molar flow rate, mol min^{-1}; *V* and *L* stand for vapor and liquid water, respectively; in and out for inlet and outlet of the cell; *F* for Faraday water; An and Ca for anode and cathode; and xo for crossover through the GDL.

The water balance results are shown in Fig. 12(b): all Faraday water flowed out through the cathode electrode, and there was no neat water flux through the membrane to the anode side at 45 °C. Water partially flowed out through the cathode electrode and the rest crossed though the membrane to the anode side and flowed out through the anode electrode at 60 °C. Some of the anode water went through the membrane to the cathode side and flowed out with the Faraday water through the cathode GDL at 80 °C. Assuming the liquid and the vapor water reach equilibrium at the interface of the cathode catalyst layer and GDL, the amount of liquid water that goes through the cathode GDL is estimated by subtracting the vapor flow rate using the dry air flow rate and the water vapor saturation pressure, as shown in Table 2.

Generally, the time scale of the gas phase transport of SO_2 through the GDL is approximately 0.003 s and that of the liquid water transport in the GDL and CL is approximately 0.2 s [43]. The latter value is higher than the residence time of SO_2 in the flow field, which is approximately 0.072 s. Therefore, the gas transport of the SO_2 control step is located in the liquid and solid phase, as previously stated. The liquid water content in the gas diffusion electrode as well as the solubility and the concentration of SO_2 are key parameters for the mass transport of SO_2 to the catalyst during contamination. Table 2 shows that the solubility of SO_2 in liquid water correlated negatively temperature. The SO_2 solubility in liquid water at 45 °C is approximately 2.5 times that at 80 °C, which provide an increased mass transfer driving force. However, the liquid water flow rate through the cathode GDL at 45 °C is approximately 5.9 times of that observed at 80 °C, which results in much more liquid water in the catalyst layer (CL) at 45 °C. This result suggests that the Nafion/water film was much thicker at 45 °C than at 80 °C. The increased thickness increased the SO_2 transport distance assuming a similar water distribution on the surface across the MEA area. The increase in the transport distance is much larger than the increase of the mass transfer driving force at 45 °C. Based on Fick's first law, the mass transport of SO_2 to the catalyst at 45 °C should be slower than that at 80 °C. Thus, a smaller fraction of the injected SO_2 flow would have access to the catalyst layer. During the cell performance degradation period, the decreased SO_2 mass transport flow rate would slow the impact of the contamination on the cell performance. Therefore, this mass transport effect should contribute to the slower cell performance degradation and the delay in the SO_2 contamination process at lower cell temperatures, as shown in Figs. 1 and 2. The thicker Nafion/water film in the CL at 45 °C also explains the larger oxygen mass transport time constant obtained by the EIS analysis (Table 1).

Additionally, some of the dissolved SO_2 can dissociate into HSO_3^- in the liquid water in the cathode electrode when it is diffusing from the flow field to the cathode catalysis layer. This dissolved SO_2 may also be flushed out by the liquid water, as

Table 2
The measured and estimated parameters for the semi-quantitative analysis of the water effect on the contamination process.

Parameter	45 °C	60 °C	80 °C
H_2O flow rate through cathode CL [g min^{-1}]	0.166	0.159	0.219
Liquid H_2O flow rate through cathode GDL [g min^{-1}]	0.142	0.102	0.024
SO_2 solubility in liquid H_2O [mol kg^{-1}_{H2O} bar^{-1}]	0.76	0.50	0.31
SO_2 flow rate in liquid H_2O [mol min^{-1}]	3.02E-10	1.33E-10	1.49E-11
HSO_3 dissociation constant [mol L^{-1}]	8.73E-3	6.61E-3	4.74E-3
HSO_3^- flow rate in liquid H_2O [mol min^{-1}]	2.30 E-8	1.08 E-8	1.31E-9
Scavenged fraction of SO_2 in different compounds [%]	26.2	12.3	1.49

discussed in the literature [43]. The scavenging can affect the real concentration of SO_2 in the gas phase. Therefore, the SO_2 compounds flow rates in liquid water are also considered based on the solubility and dissociation constant of SO_2 at different temperatures to understand the water effect on the contamination processes. The SO_2 flow rate in liquid water at the cell outlet was estimated by assuming equilibrium for both the dissolution saturation and dissociation states. Table 2 shows that the SO_2 compounds flow rates in liquid water increased as the cell temperature decreased. The rate of liquid water-scavenged SO_2 is approximately 1.49%, 12.3% and 26.2% of the SO_2 injection flow rate ($8.89 * 10^{-8}$ mol min^{-1}) at 80, 60 and 45 °C, respectively. This scavenging effect also contributes to the delay in the SO_2 contamination process at lower cell temperature as shown in Figs. 1 and 2. Furthermore, lower temperature caused stronger SO_2 adsorption based on the CV analysis, as discussed in Fig. 8 and Section 3.2.2. This increase should result in increased cell performance losses at steady state. Nevertheless, similar performance losses were observed at steady state for all temperatures. This finding might be explained by the scavenging effect, which decreases the real concentration of SO_2 in the electrode and decreases the performance loss at steady state. In other words, the stronger SO_2 adsorption effect on the cell performance loss was compensated by the liquid water scavenging effect at low cell temperatures.

4. Conclusions

The effects of the cell operating temperature on sulfur dioxide (SO_2) contamination in PEMPEMFCs were investigated with 2 ppm SO_2 in the cathode. The operating temperature significantly influences the cell voltage degradation processes, CV recovery and the degradation processes caused by a second exposure. The second degradation stage was delayed by decreasing the cell temperature due to the liquid water scavenging and mass transport effect. The degree to which reversible and irreversible poisoning degradations can be recovered strongly depended on the cell temperature. As the cell temperature increased, the self-recovered performance increased but the total recovered performance decreased. At low cell temperature, self-recovery yielded only negligible results, but full recovery of the cell performance was achieved by CV scanning. The EIS and CV analysis of the electrodes implied that the potential-dependent poisoning process was delayed and the desorption of the sulfur species on Pt/C was inhibited at low cell operating temperature. The SO_2 crossover from the cathode to the anode side was also restrained at low cell temperature due to the high water content in the MEA and low gas permeability of the membrane.

In summary, the low cell temperature reduced the cell performance degradation during the first and transient periods and showed similar performances to those at the other temperatures at the steady poisoning state, despite the strong adsorption of the sulfur species. The operating temperature affects the SO_2 contamination process by influencing the SO_2 mass transport and the SO_2 desorption during the performance recovery. These findings will provide helpful information to understand the SO_2 poisoning process and develop mitigation and recovery strategies.

Acknowledgments

The authors gratefully acknowledge funding from the Office of Naval Research (ONR) under Award Number N00014-10-1-0310 and the Hawaiian Electric Company for their ongoing support to the operations of the Fuel Cell Test Facility.

References

[1] W.H.J. Hogarth, J.C.D. da Costa, G.Q.M. Lu, J. Power Sources 142 (2005) 223–237.
[2] R. Borup, et al., Chem. Rev. 107 (2007) 3904–3951.
[3] J. St-Pierre, Air impurities, in: F.N. Büchi, M. Inaba, T.J. Schmidt (Eds.), Polymer Electrolyte Fuel Cell Durability, Springer, New York, 2009, pp. 289–321.
[4] J. Zhang, H. Wang, D.P. Wilkinson, D. Song, J. Shen, Z.S. Liu, J. Power Sources 147 (2005) 58–71.
[5] X. Cheng, Z. Shi, N. Glass, L. Zhang, D. Song, Z. Liu, H. Wang, J. Shen, J. Power Sources 165 (2007) 739–756.
[6] S. Dorn, Y. Zhai, R. Rocheleau, Electrochem. Soc. Trans. 28 (23) (2010) 183–191.
[7] J.M. Moore, P.L. Adcock, J.B. Lakeman, G.O. Mepsted, J. Power Sources 85 (2000) 254–260.
[8] R. Mohtadi, W.K. Lee, J.W. Van Zee, J. Power Sources 138 (2004) 216–225.
[9] F. Jing, M. Hou, W. Shi, J. Fu, H. Yu, P. Ming, B. Yi, J. Power Sources 166 (2007) 172–176.
[10] Y. Nagahara, S. Sugawara, K. Shinohara, J. Power Sources 182 (2008) 422–428.
[11] J. Fu, M. Hou, C. Du, Z. Shao, B. Yi, J. Power Sources 187 (2009) 32–38.
[12] O.A. Baturina, K.E. Swider-Lyons, J. Electrochem. Soc. 156 (2010) B1423–B1430.
[13] Y. Garsany, B.D. Gould, O.A. Baturin, K.E. Swider-Lyons, Electrochem. Solid-State Lett. 12 (2009) B138–B140.
[14] B.D. Gould, O.A. Baturina, K.E. Swider-Lyons, J. Power Sources 188 (2009) 89–95.
[15] Y. Zhai, G. Bender, S. Dorn, R. Rocheleau, J. Electrochem. Soc. 157 (2010) B20–B26.
[16] B.D. Gould, G. Bender, K. Bethune, S. Dorn, O.A. Baturina, R. Rocheleau, K.E. Swider-Lyonsa, J. Electrochem. Soc. 157 (2010) B1569–B1577.
[17] J. Zhai, M. Hou, H. Zhang, Z. Zhou, J. Fu, Z. Shao, B. Yi, J. Power Sources 196 (2011) 3172–3177.
[18] Y. Zhai, K. Bethune, G. Bender, R. Rocheleau, J. Electrochem. Soc. 159 (2012) B524–B530.
[19] Y.M. Sun, D. Sloan, D.J. Alberas, M. Kovar, Z.J. Sun, J.M. White, Surf. Sci. 319 (1994) 34–44.
[20] U. Kohler, H.W. Wassmuth, Surf. Sci. 126 (1983) 448–454.
[21] C. Quijada, J.L. Vázquez, J.M. Pérez, A. Aldaz, J. Electroanal. Chem. 372 (1994) 243–250.
[22] St. Astegger, E. Bechtold, Surf. Sci. 122 (1982) 491–504.
[23] U. Kohler, H.W. Wassmuth, Surf. Sci. 117 (1982) 668–675.
[24] K. Wilson, C. Hardacre, C.J. Baddeley, J. Ludecke, D.P. Woodruff, R.M. Lambert, Surf. Sci. 372 (1997) 279–288.
[25] A.Q. Contractor, H. Lal, J. Electroanal. Chem. 93 (1978) 99–107.
[26] X. Lin, W.F. Schneider, B.L. Trout, J. Phys. Chem. B. 108 (2004) 250–264.
[27] S.E. Lyke, S.H. Langer, Sep. Technol. 2 (1992) 13–18.
[28] M. Polck, L. Wilde, J. Haase, B. Brena, G. Comelli, G. Paolucci, Surf. Sci. 381 (1997) L568–L572.
[29] P. Zebisch, M. Stichler, P. Trischberger, M. Weinelt, H.P. Steinruck, Surf. Sci. 371 (1997) 235–244.
[30] K. Punyawudho, S. Shimpalee, J.W. Van Zee, ECS Trans. 25 (1) (2009) 1289–1298.
[31] C. Quijada, A. Rodes, J.L. Vfizquez, J.M. P&ez, A. Aldaz, J. Electroanal. Chem. 394 (1995) 217–227.
[32] O.A. Baturina, B.D. Gould, A. Korovina, Y. Garsany, R. Stroman, P.A. Northru, Langmuir 27 (2011) 14930–14939.
[33] R.M. Spotnitz, J.A. Colucci, S.H. Langer, Electrochim. Acta 28 (1983) 1053–1062.
[34] M.J. Foral, S.H. Langer, J. Electroanal. Chem. 246 (1988) 193–205.
[35] I.R. Moraes, M. Weber, F.C. Nart, Electrochim. Acta 42 (1997) 617–625.
[36] Y. Garsany, O.A. Baturin, K.E. Swider-Lyons, J. Electrochem. Soc. 154 (2007) B670–B675.
[37] Y. Garsany, O.A. Baturin, K.E. Swider-Lyons, J. Electrochem. Soc. 156 (2009) B848–B855.
[38] M.A. Hickner, N.P. Siegel, K.S. Chen, D.S. Hussey, D.L. Jacobson, M. Arif, J. Electrochem. Soc. 155 (2008) B294–B302.
[39] S. Jomori, N. Nonoyama, T. Yoshida, J. Power Sources 215 (2012) 18–27.
[40] R. Mohtadi, W.K. Lee, S. Cowan, J.W. Van Zee, M. Murthy, Electrochem. Solid-State Lett. 6 (2003) A272–A274.
[41] R. Mohtadi, W.-K. Lee, J.W. Van Zee, Appl. Catal. B 56 (2005) 37–42.
[42] K. Broka, P. Ekdunge, J. Appl. Electrochem. 27 (1997) 117–123.
[43] B. Wetton, J. St-Pierre, Electrochem. Soc. Trans. 50 (2) (2013) 649–657.